An Earth Centered Mapping of the Residual Background in the Fermi LAT

FINAL REPORT FOR NASA GRANT NNX09AT69G
Period of performance: 09/01/09-8/31/10

PI: Jonathan F. Ormes
Department of Physics and Astronomy
2112 E. Wesley Ave.
University of Denver
Denver, CO 80208
DU identification number: 36655

August 31, 2010

As indicated in the original proposal, measurement of the diffuse high-energy (>30 MeV) extragalactic isotropic gamma radiation is a key objective of the *Fermi* Large Area Telescope (LAT) (see Abdo et al., 2010a). "Is there a component of this diffuse gamma radiation that cannot be attributed to individual sources?" is an important question for understanding the baryon asymmetry of the Universe with profound consequences for cosmology (Steigman, G. 1976; Cohen, de Rujula and Glashow, 1998; Stecker, 2003) and particle physics (Kolb and Turner, 1983; Mohapatra, 2003). The most sensitive measurements prior to the launch of Fermi came from the Energetic Gamma Ray Experiment Telescope (EGRET) on the Compton Gamma Ray Observatory (CGRO) (Sreekumar, 1998). Analyses of EGRET's instrumental calibrations (Stecker, Hunter and Kniffen, 2008), and of galactic foregrounds (Strong, Moskalenko and Reimer, 2004), and solar system foregrounds (Moskalenko et al., 2008) demonstrate some of the observational challenges.

Finding a diffuse component of extragalactic gamma-rays, and other background limited measurements such as the search for a dark matter halo of gamma rays from the LMC, were thought to be limited by the ability to deal with instrumental and local backgrounds. For example, the extragalactic radiation is observed through several foreground layers of emission from intervening mechanisms:

1) Galactic diffuse radiation from cosmic rays interacting with matter in the interstellar medium and from Inverse Compton emission

from the cosmic ray electrons interacting with the low energy photons from stars and the microwave background radiation.

2) Solar system sources, including small solid bodies and Inverse Compton from the solar photon field (Moskalenko et al., 2008).

3) Very local sources of instrumental background including photons generated in the material surrounding the LAT and the Earth.

It is the 3rd of these components that was the subject of this investigation. LAT, with its large collecting power (live time fraction, effective area and viewing angle) and improved angular resolution compared to EGRET, has resolved the extragalactic sky into thousands of individual sources, and may reach a limit at which source confusion becomes a problem (Abdo et al., 2010b). At this level, the analysis will depend on detailed understanding of the instrumental background and of the local haze of photons made by galactic cosmic rays and by electrons, positrons and protons trapped or quasi-trapped in the Earth's magnetic field. These particles, interacting in species dependent ways, can produce photons in the material around the instrument that are indistinguishable within the instrument from the celestial photons being sought. While the LAT instrument design has been optimized to minimize such effects, they are not completely eliminated. The most probable mechanisms for producing locally generated photons include the following:

1) Hadrons can interact and create a gamma ray, either directly or through the decay of a secondary particle from the interaction in such a way that no charged particle is seen, thereby making no signal that can be used to veto the event.

2) Trapped positrons, found (Voronov, 1991; Alcaraz et al. 2000, Mikhailov, 2002) to be more abundant near the equator, can annihilate into two photons in the material in front of the LAT, material that is there to protect the instrument against micro-meteorites and thermal extremes.

3) Both positively and negatively charged electrons can transfer most of their energy to photons via Bremsstrahlung interactions in the same material, leaving a charged particle without enough energy to

be detected and resulting in a gamma-ray that is not vetoed.

The GLAST (now *Fermi*) Science Requirements (Gehrels and Michelson, 1999) specify these backgrounds in total to be at the level of approximately 10% of that of the diffuse extra-galactic gamma-ray flux, as determined by EGRET (Kniffen et al., 1996).

Had they been of significant magnitude, these components of unidentifiable background would have different but characteristic patterns as a function of the satellite's orbital position and perhaps arrival direction in local geographic and/or geomagnetic coordinates (McIlwain L and B, and local field direction). The components listed above are distributed as follows:

1) Trapped albedo positrons dominate near the geomagnetic equator (Alcaraz et al. (2000) and others (Derome et al., 2001; Dmitriev, 1998; Zuccon, 2003)).
2) Simulations (Honda, 2009) show that albedo electron and positron populations peak near the South Atlantic anomaly and have characteristic spatial distributions in latitude and longitude.
3) The flux of galactic cosmic rays varies with the well-known and well-understood local geomagnetic cutoff, including east-west effects.
4) The flux of trapped cosmic ray protons depends on the local zenith angle as well as latitude and probably longitude (Zuccon, 2003 and references therein).
5) The distribution of instrumental background rate will depend on its origin.

The aim of this proposal was to characterize the LAT background as a function of orbital position. High galactic latitude (b>30 degrees) data were selected for use in the analysis. As I shall show, the data, when integrated over long times to average out orbital variations in effective area, allow this data to be considered a quasi-standard candle. Eighteen months of data allowed precise measurements of this diffuse emission from various points on the orbit. I will describe in the remainder of this document, the approach to the analysis, show how time variations in flux are dealt with, show some higher background regions around the South Atlantic Anomaly, and show how the flux varies with the location on orbit from which the observations were made.

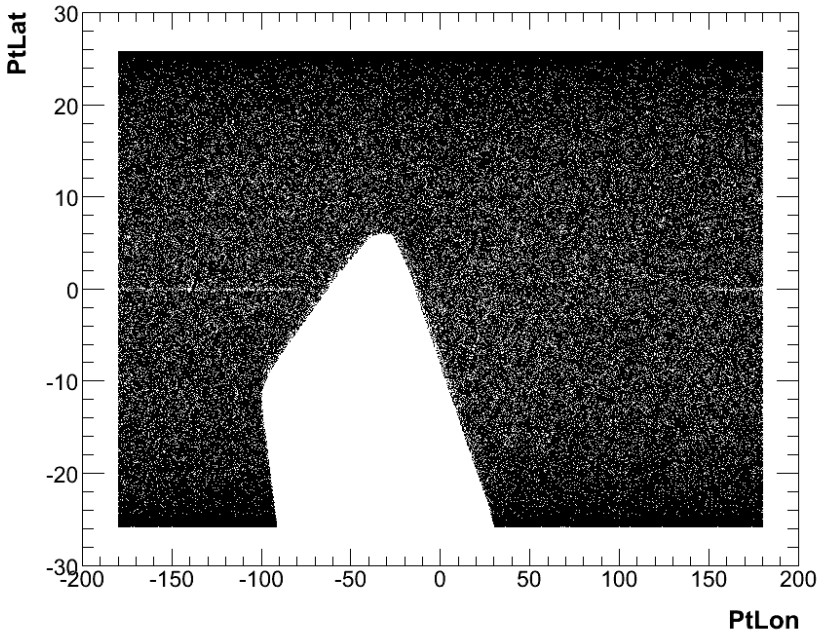

Figure 1: Mapping of the location of the satellite for selected events. No events were taken during passage through the SAA as defined for standard analysis of Fermi data. Note the streak at zero latitude where the run clock was restarted each orbit.

—

We will show there are regions in the orbital parameter space where background is somewhat less, particularly at low energies. Such regions that can be used as "windows" in the wall of local haze through which more sensitive background limited observations can be made. Because the background sources have different spectra (e.g. galactic cosmic ray protons vs. trapped protons), the optimal locations are different geographically for different energies. We shall show that the best regions for 0.05 to 300 MeV energies are those to the north and east of the South Atlantic Anomaly (SAA) in the northern hemisphere.

The approach was to use 18 months of high latitude data as a "Standard Candle" to search for flux variations correlated with geographic or geomagnetic coordinates. The data set is described in detail in the presentation given at GSFC on June 16, 2010 (Ormes, 2010). As seen in Figure 1, a plot of the rate as a function of geographic latitude and longitude shows data was not taken in the SAA. This plot also shows a streak of missing data at the equatorial crossings from longitude about

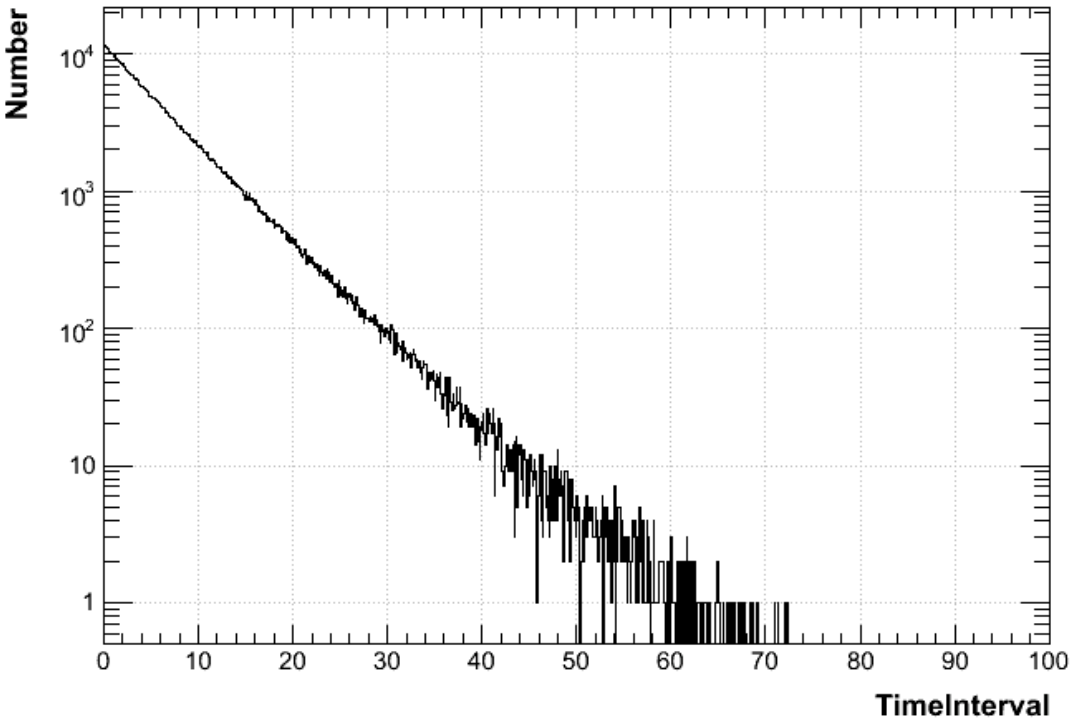

Figure 2: Distribution of intervals between counts in the sample used. The units are seconds. Any event with a time interval greater than 75 seconds was excluded from analysis and clocking was restarted. This removed anomalies due to SAA crossings and other occasional timing errors.

—

140^o to -90^o. This corresponds to data missed as the satellite processes "runs" that are initiated either on exit from the SAA or, when there is no intersection of the orbit with the SAA, at the equatorial crossing.

I used the data itself to determine rates at given locations. Gamma-rays were selected using the standard analysis tools. The diffuse class of gamma rays was used for making the data set; this data includes all events that are recognized as photons by the analysis, including both celestial photons as well as any local background photons or "apparent photons". Live and dead times were determined for any observational location. Each LAT event is time tagged and numbered, but the rate of selected events was small compare to the total event rate. Elapsed time between photons was obtained by accumulating time differences between selected events. The number of intervening events was obtained from the differences in the event numbers assigned to the selected events. Dead

time was found using 26.5 μs/event time a factor of 1.16 to account for the larger dead time of the interspersed calibration events. Another check on the use of rate data was to make sure the resulting interval distribution reflected the expected rate and exponential shape. The result is shown in Figure 2.

The dead time is further corrected for an effect not accounted for in the standard analysis. When the rate is higher, the probability that an accidental coincidence occurred during the data accumulation and event processing time goes up. This is an energy dependent effect and is corrected using a prescription developed by Eric Charles (2009) and incorporated in the estimation of live time as given in the FT2 files. The correction is rate and energy dependent, so at high latitude, where the cutoff is lower the effect is increased. This was important because the background we are looking for could be masked/enhanced by our failure to properly account for such an effect. Details of the implementation of the correction are given in Ormes (2010). I refer to this correction as a 2^{nd} order dead-time correction.

The data set included 48×10^6 events taken from August 10, 2008 until February 12, 2010. Pass 6 Diffuse class events[1] were used then further trimmed using the background rejections known as ExtraDiffuse and DataClean as described in Abdo et al. (2010a). Photons with energy from 50 MeV to 10 GeV were selected. Additional cuts assured the Earth was not in the field of view (local zenith angle of arrival < 100 degrees – Earth horizon is at 110 degrees) and events with angles of incidence on the detector >60 degrees were removed.

For studies using magnetic locations on the Earth, the geomagnetic latitude, lambda, was used. Lambda uses the McIlwain B and L coordinates[2] to take into account the location of the center magnetic dipole from the geographic equator and spin axis and the non-dipole terms in the Earth's magnetic field. An algebraic sign was assigned to this variable so north and south could be distinguished for the purposes of this study. The definition of this parameter and the location of the equator are given (Ormes, 2010, p20).

[1] http://www-glast.slac.stanford.edu/software/IS/glast_lat_performance.htm
[2] http://www.spenvis.oma.be/spenvis/help/background/magfiels/bl.html

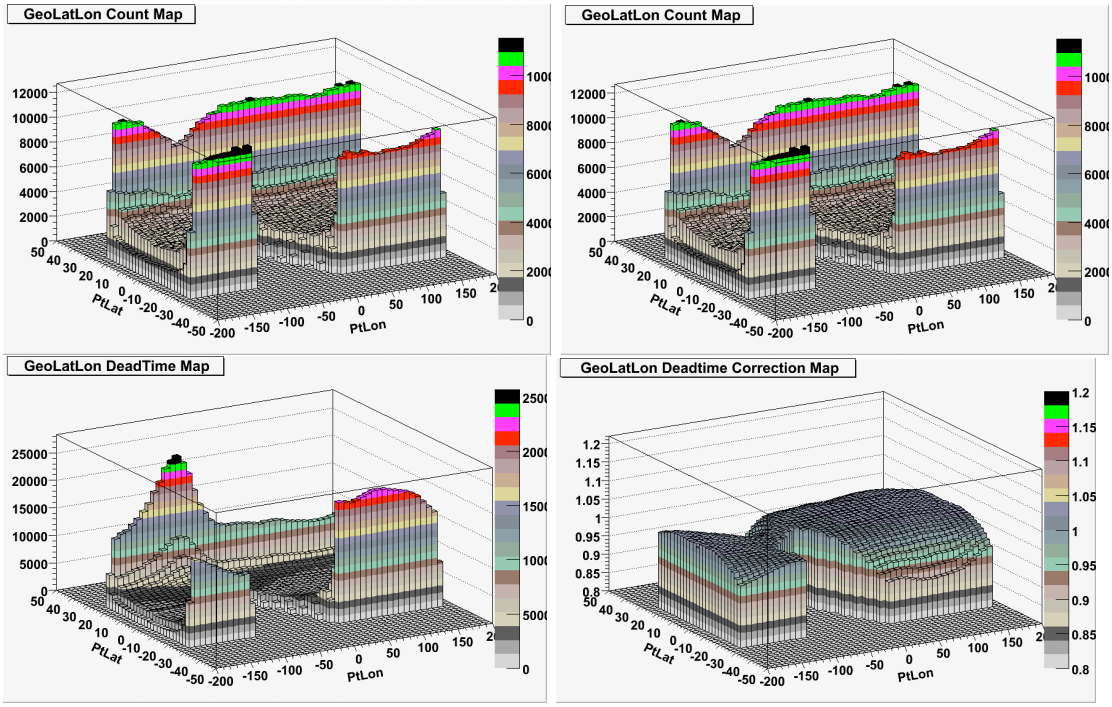

Figure 3: Two dimensional maps of counts, time, dead-time, and deadtime correction as a function of geographic latitude and longitude.

—

The next step was to evaluate the constancy of the flux. On short time scales (e.g. a few orbits), this patch of sky moves around on the LAT field of view as the satellite moves in the orbit, so a plot or rate vs. time shows passes through the SAA, and other modulations of +/-50%. Large changes are seen on 200 s integration times. At 20-100 ks time scales variations are reduced to +/- 10%. Data dropouts are visible when the satellite was in other than normal scanning modes; such time periods were removed (Ormes, 2010).

How standard is this candle? I then subdivided the orbital precession period of 4.61 x 10^6 s into 8 equal phase bins. Deviations from the mean rate were 2.54%, 2.50%, 0.83%, -0.93%, -1.95%, -2.56%, -1.00%, and 0.35% for these 8 bins. So there are variations of +/-2.6% associated with the orbital precession period. I compared north and south geomagnetic latitudes. When the satellite rocks towards the north and then the south, it will observe different parts of the sky at different phases of the precession. The overall rate is higher by 2.8% when the spacecraft is at

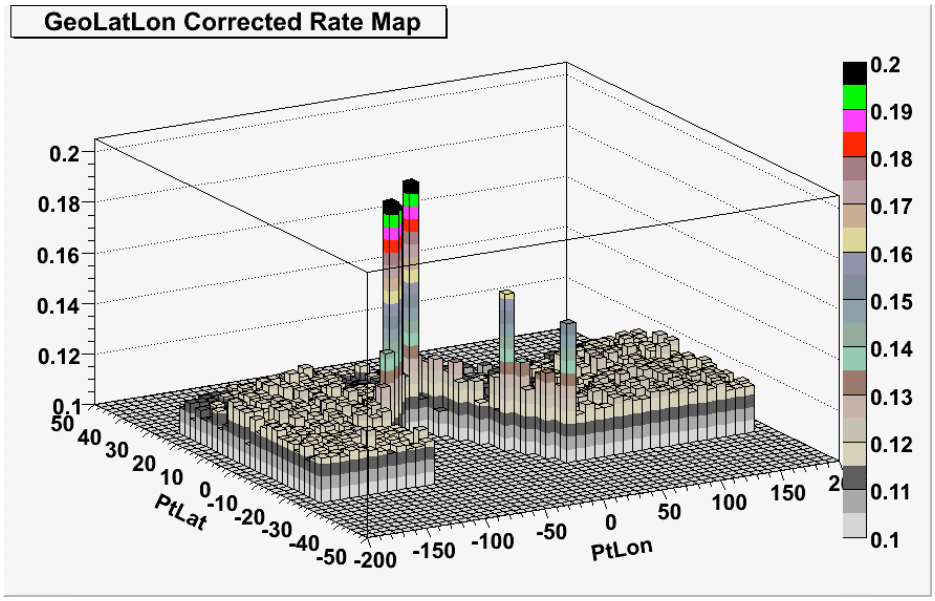

Figure 4: Map of rates near the South Atlantic Anomaly. Some bins show rates double the normal indicating background of order the level of the signal in such bins.

—

south geomagnetic latitude. The expected phase difference of 180 degrees is seen, and the amplitude, is increased:

North: 4.04% 1.30% -3.24% -7.16% -6.72% -0.20% 5.87% 5.58%

South: 1.25% 3.56% 4.38% 4.57% 2.24% -4.62% -7.17% -4.24%

This gives a feeling for the amplitude of variations of the high latitude diffuse as observed during different times. By integrating over more than 10 precession periods, such effects are reduced to the 1-2% of the count rate. Since typical rates are 0.1 Hz, this corresponds to an effective rate of +/- 1-2 x 10^{-3} Hz. Larger rate variations are evidence for real systematic effects.

With these preliminary steps taken, rate maps were made. Figure 3 shows four such maps to illustrate the process. Shown in this figure are maps of (1) counts vs. geographic latitude and longitude, (2) time spent by the satellite collecting these events, (3) a corresponding map of dead time and (4) a dead time correction map. The bins in these figures are 2 degrees

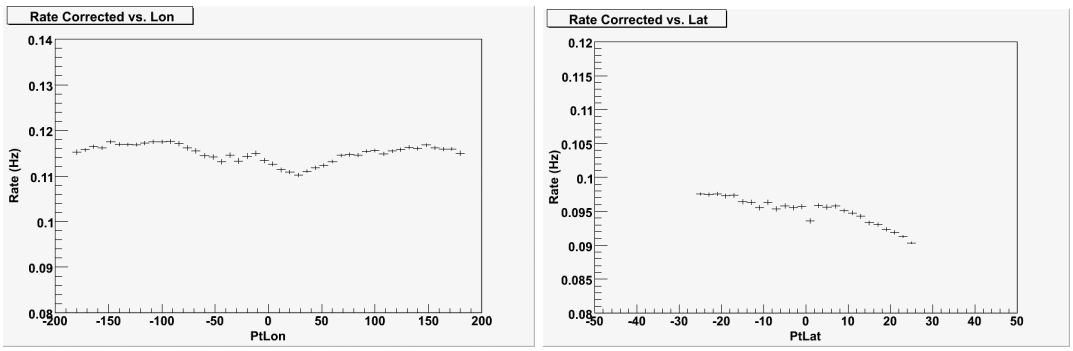

Figure 5: Rate profiles as a function of geographic longitude (left) and latitude (right).

—

wide in latitude and 8 degrees wide in longitude.

Note that the orbit makes a sinusoid in geographic coordinates so the largest number of counts and the longest times come at the orbital extremes of latitude. Note also the dip in counts and increase in dead time in the north at longitude about -80 degrees. This is the point in the orbit where the geomagnetic cutoff is least and the rate of galactic cosmic rays is highest. This results in a corresponding structure in the dead time correction map. A rate map is constructed by dividing the counts (e.g. Figure 3a) in a given bin
by the elapsed_time - corrected_dead_time for the same bin (e.g. Figure 3d).

Figure 4 shows such a rate map. Clearly there are anomalous rates found near the boundary of the SAA, which was defined to keep the counting rate of the detectors responding to charged particles in the radiation belt to a level where the data would be unaffected. However, the data taken near the SAA can have greatly enhanced background. Overall, such background would not affect a flux measurement too much because the counts involved are not large, but for background sensitive measurements, an expanded region around the SAA should be excluded. For the purposes of the remainder of this study, I excluded events that were within 2 bins of the defined SAA.

Preliminary work was done using one-dimensional plots of resulting rates. Figure 5 shows such profiles as a function of longitude and latitude.

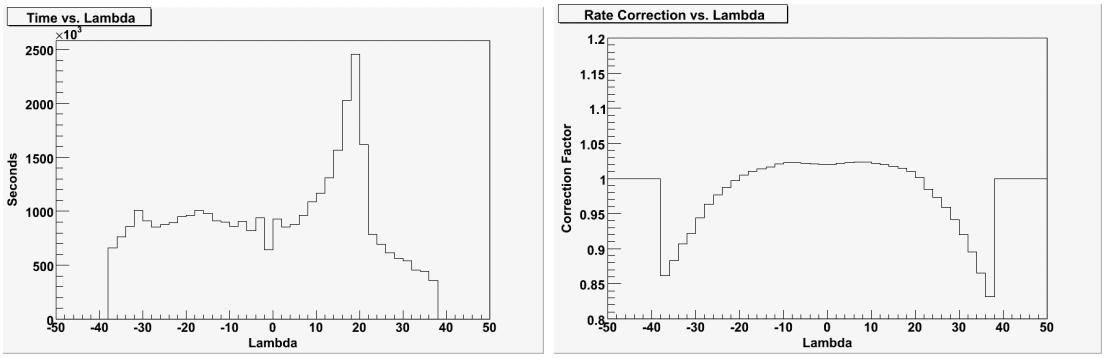

Figure 6: The left panels shows the distribution of time spent by satellite and the right panel shows the dead-time correction as functions of geomagnetic latitude, lambda.

—

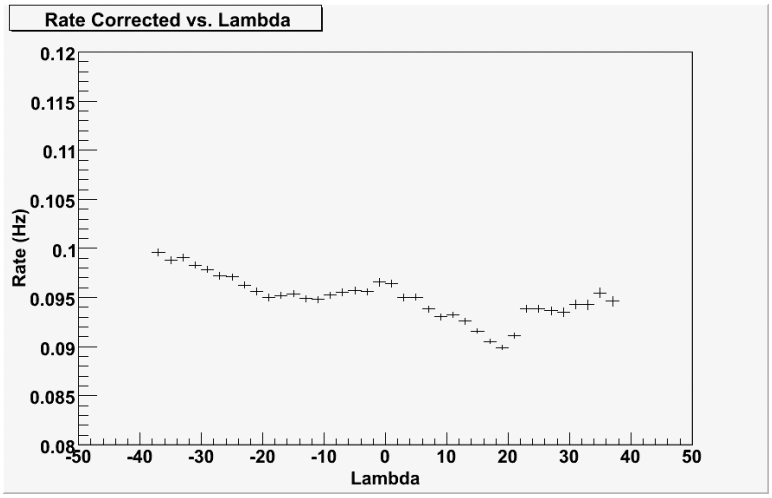

Figure 7: Rate as a function of magnetic latitude.

—

It is more interesting to consider variations with the lambda variable discussed above because the variable is simply related to the geomagnetic cutoff and hence to the rate of galactic cosmic rays. Figure 6a shows the distributions of where the satellite spent its time in this coordinate. Figure 6b shows the correction of the rate for dead time and superimposed loss of events due to chance coincidences as discussed above. As noted above, I refer to the latter as the second order dead-time correction. Note both corrections are largest at the orbital extremes.

The dead-time corrected rate vs. the magnetic latitude is shown in Figure 7. The overall latitude profile (signed lambda) shows some difference

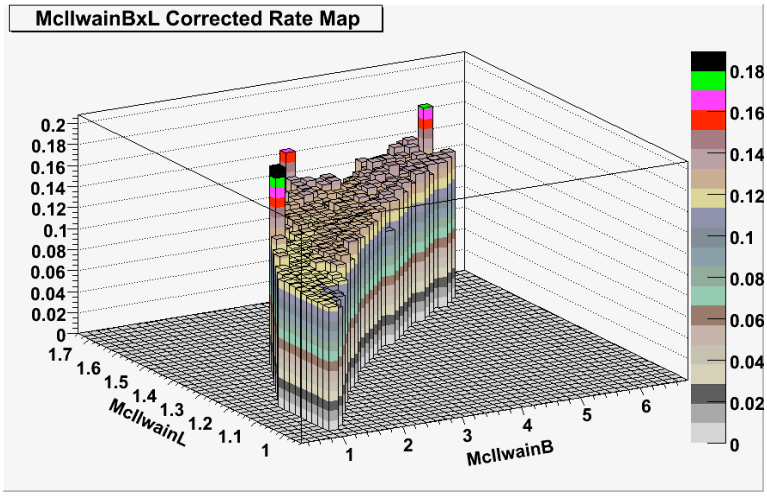

Figure 8: Rate map as a function of McIlwain B and L coordinates.

—

north to south and a general trend with increasing latitude. Ideally, such a profile should show no variation, but a trend of decreasing rate as magnetic latitude increases is seen, and there are further modulations which appear to be statistically significant.

To further understand this modulation, plots were made using McIlwain B and L coordinates separately for both negative and positive lambda. These variables appear to organize the data quite nicely as shown in Figure 8.

Figure 9 shows these data without the 2nd order dead-time correction for chance coincidences. Standard *Fermi* Large Area Telescope analysis uses an energy dependent prescription for the 2nd order dead-time correction developed by the LAT team. Figure 10 shows the same four plots as in Figure 8 but with the 2nd order correction included. Note that the corrections reverse the trends with latitude. I found that a correction reduced by 30% made these plots independent of the McIlwain parameters as shown in Figure 11, again for the same four plots as in Figure 9.

This reduced version of the 2nd order dead-time correction appears to correct rates properly for instrumental and analysis effects and will be used in the remainder of this report. Note that the correction is energy dependent.

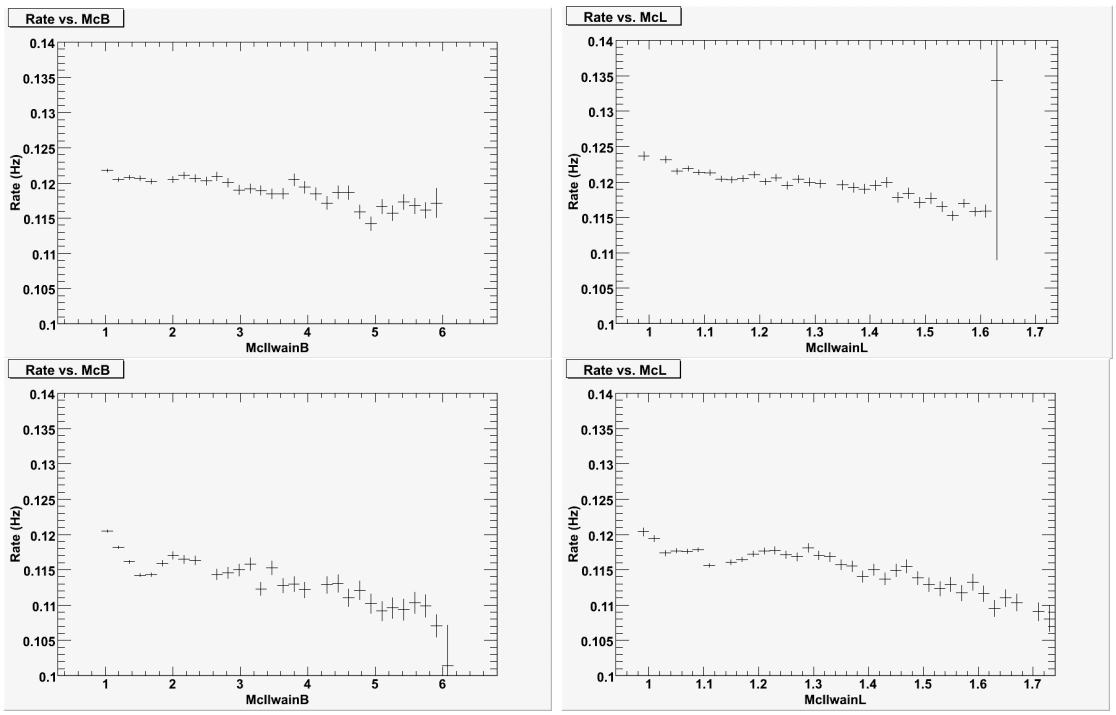

Figure 9: Rate as a function of McIlwain B and L parameters for rates without 2nd order dead time correction for chance coincidences. Upper two panels are for negative magnetic latitudes and the lower two panels are for positive magnetic latitudes (as defined using the signed magnetic latitude variable lambda). The left panels are for McIlwain B and the right panels are for McIlwain L.

—

Once the rates of these high latitude diffuse gamma rays are corrected to be independent of observation time (using very long integrations) and of McIlwain B and L parameters (as proxies for count rate effects), we can be confident that any residual effects are due to either celestial photon rates or local background effects. Because the satellite orbit is most simply characterized using geographic coordinates they can most easily be understood; so we use geographic coordinates for the presentation of the results. The results of the analysis are shown in Figure 12 for the energy range 31.6 MeV to 10 GeV.

A region of reduced rate is clearly seen to the north and east of the SAA. The location of this region is not correlated with the region of highest rate as would be expected if a mistake had been made in the dead-time

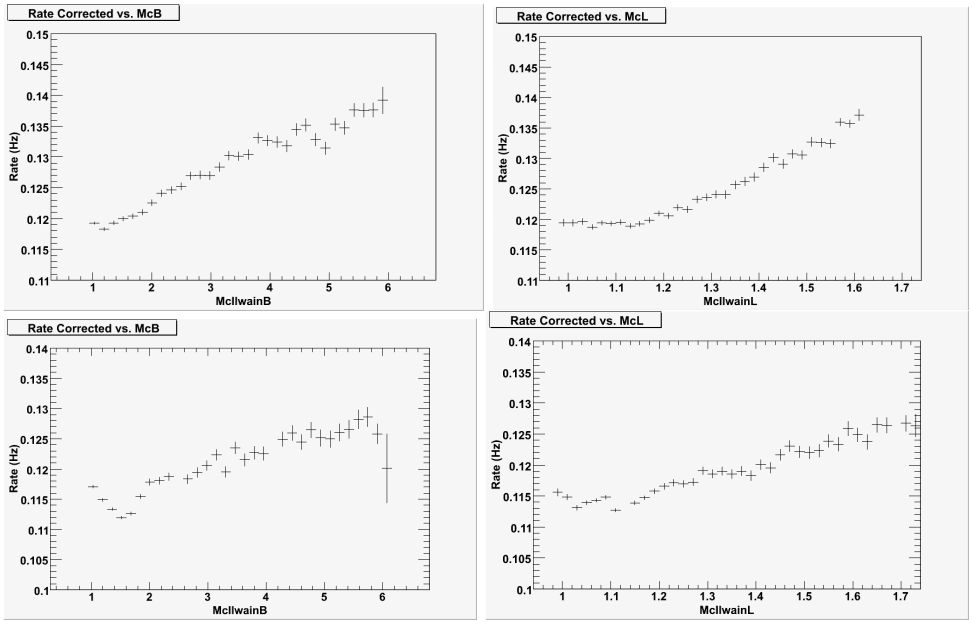

Figure 10: Rate as a function of McIlwain B and L parameters for rates with standard 2nd order dead time correction for chance coincidences. The four panels are as described in Figure 9.

—

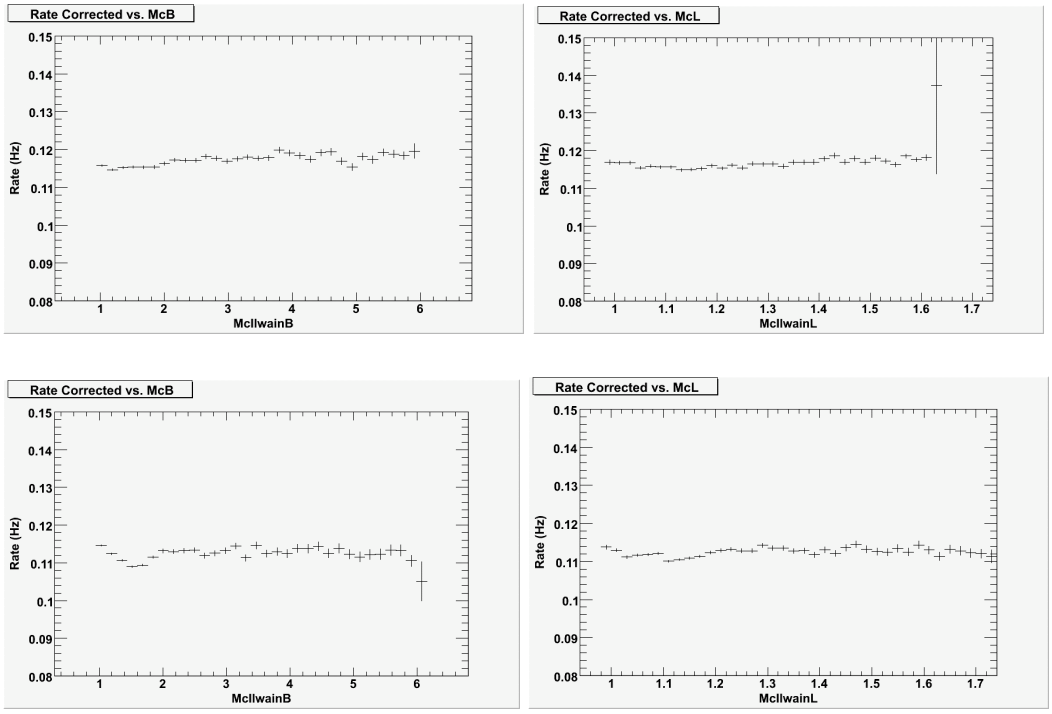

Figure 11: Rate as a function of McIlwain B and L parameters for rates with the 2nd order dead time correction for chance coincidences reduced by 30%. The four panels are as described in Figure 9.

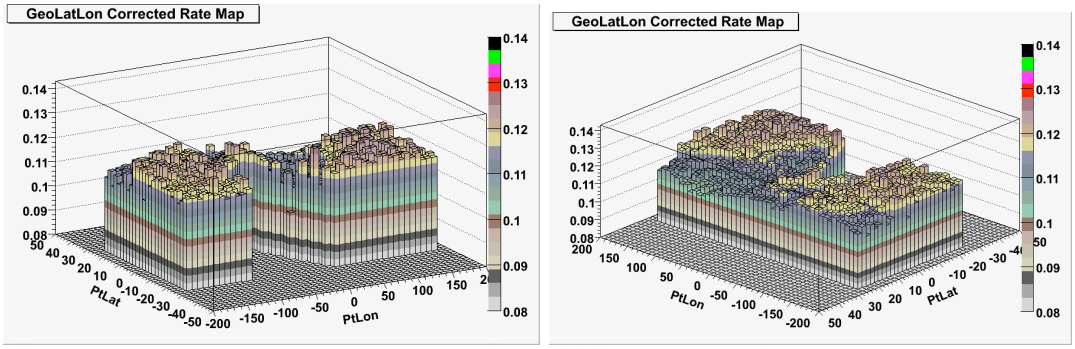

Figure 12: Rate contour map of the high latitude sky as seen from different places on the orbit as function of geographic coordinates. The contour on the right is seen from the south as the SAA region is clearly visible. The right hand panel is rotated so the map is seen from the northwest. The statistical precision in a typical bin is less than 2%. Bins with fewer than 100 counts were eliminated.

—

correction.

Figure 13 shows this region for different energy bands. The rate is different in the different bands, and the regions change shape. For example, in the highest energy band (1.77 – 10 GeV) the highest latitudes appear to have the lowest rates. On the other hand, in the low energy band (31.6-316 MeV) the rate is lowest to the northeast of the SAA. All three bands show some high rate bins at the edge of the SAA in spite of the expanded region used to eliminate such effects. Note that for the highest energy range, the statistical fluctuations from bin to bin are starting to show.

I have applied this analysis to a preliminary version of the Pass 7 analysis in which the 2nd order dead-time correction is simulated by overlaying chance coincidence events at random on top of good events. This analysis is in process, but a preliminary result is shown in Figure 14. The effect is clearly present in the data.

Simulation of >200 MeV particles at 500 km altitude from cosmic ray nuclei interacting in the atmosphere were provided by Morihiro Honda (Honda, 2009, 2007 and Sanuki, 2007). These computations were initiated to understand the flux of atmospheric neutrinos and *Pamela* data.

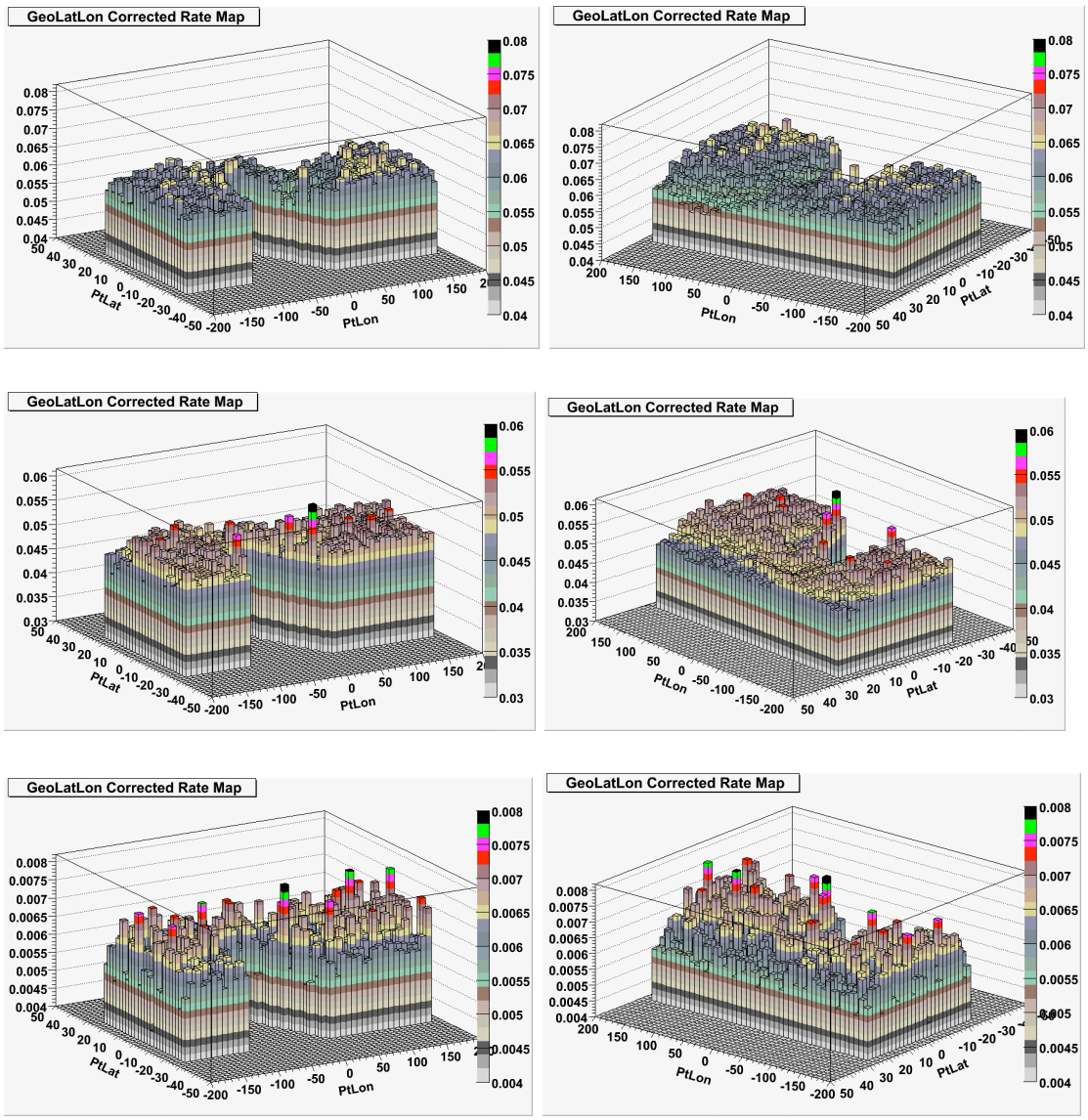

Figure 13: Same as Figure 12 for three different energy bands (MeV): top, 31.6-316; middle, 316-1770; bottom, 1770-10,000.

—

Figures 16 and 17 show the modeled distributions for secondary or Earth albedo protons and for negative and positively charged electrons. There might be an indication of a correlation with the map in Figure 17 (top) that shows a high flux of electrons to the west of the SAA, but nothing appears to correlate with the positrons. The best qualitative correlation is with the maps of nuclei including the cosmic ray flux itself as seen in Figure 18, but it is not correlated with the highest energy map given in the bottom panel of Figure 13.

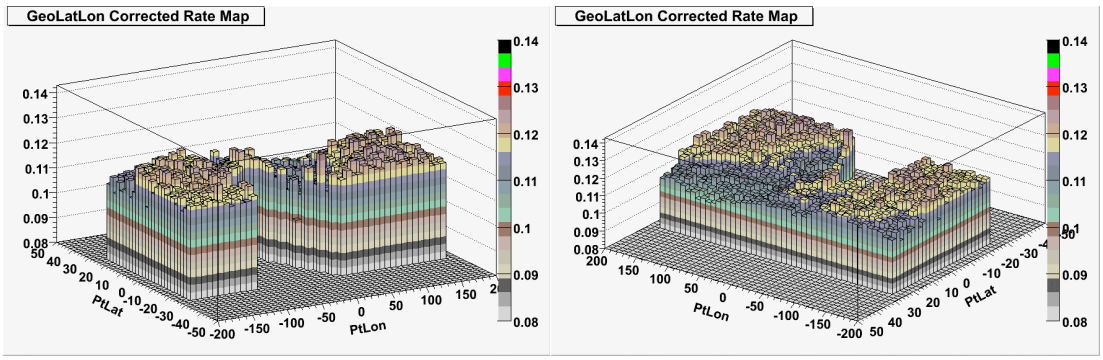

Figure 14: Same as Figure 12, but using a preliminary version of an improved analysis (Pass 7.2).

—

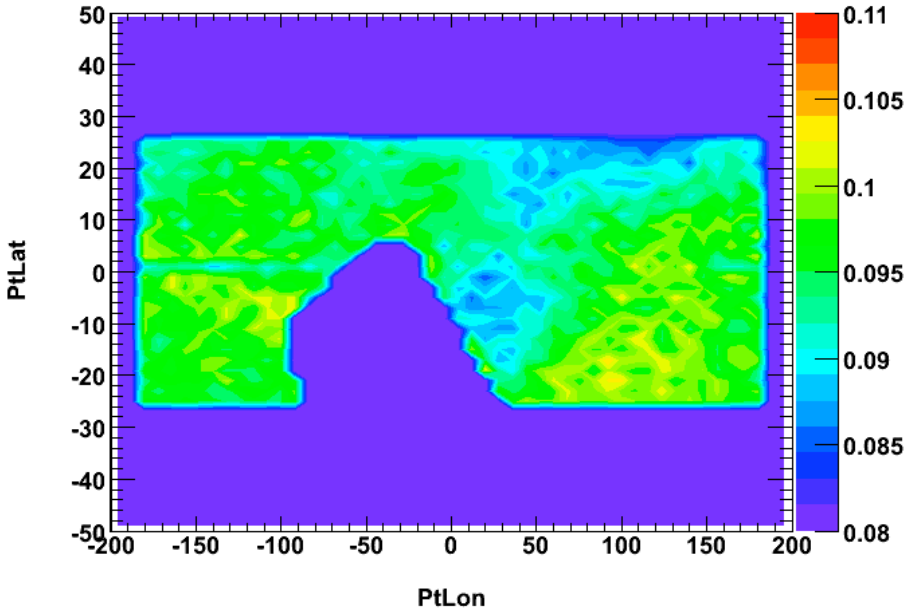

Figure 15: Contour maps of rates as in Figure 12.

—

For the purpose of comparing spectra from the different rate zones, I divided the map shown in Figures 12 and 15 into three rate regions labeled simply low, medium and high. Figure 19 shows the locations of these three rate regions. The orientations of the maps are chosen so their outlines are most easily seen. Figure 20 shows the relative rate spectra, normalized to the average rate spectrum, for data taken from these three different regions.

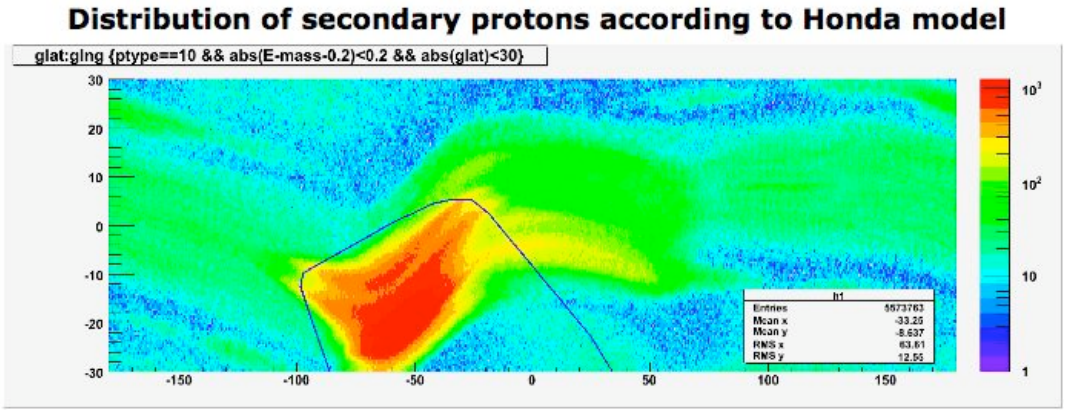

Figure 16: Distribution of secondary protons from interactions of cosmic ray nucleons with the Earth's atmosphere.

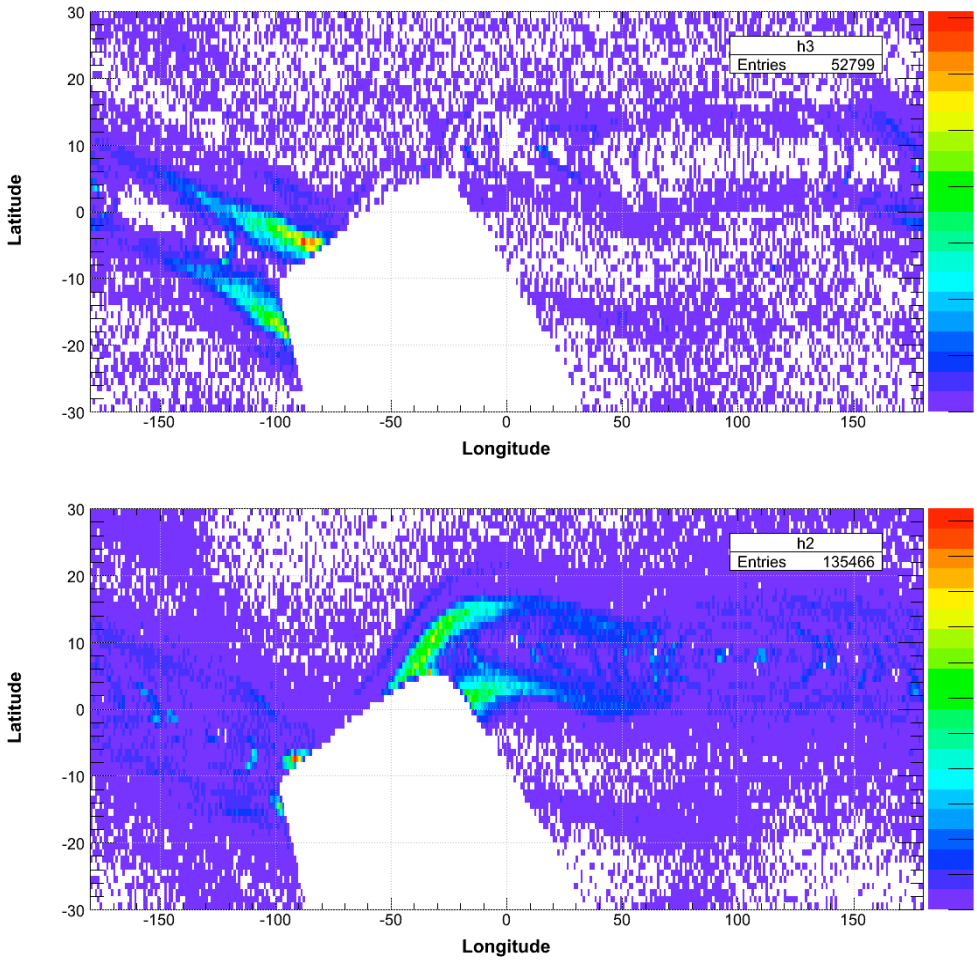

Figure 17: Distribution of secondary positrons (top panel) and electrons (bottom panel) from interactions of cosmic ray nucleons with the Earth's atmosphere.

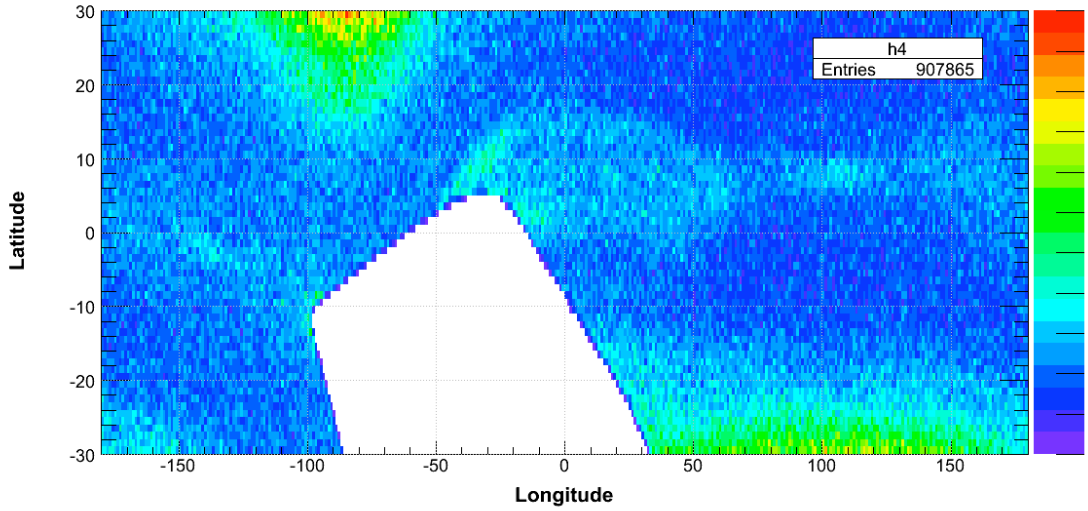

Figure 18: Distribution of nucleons.

—

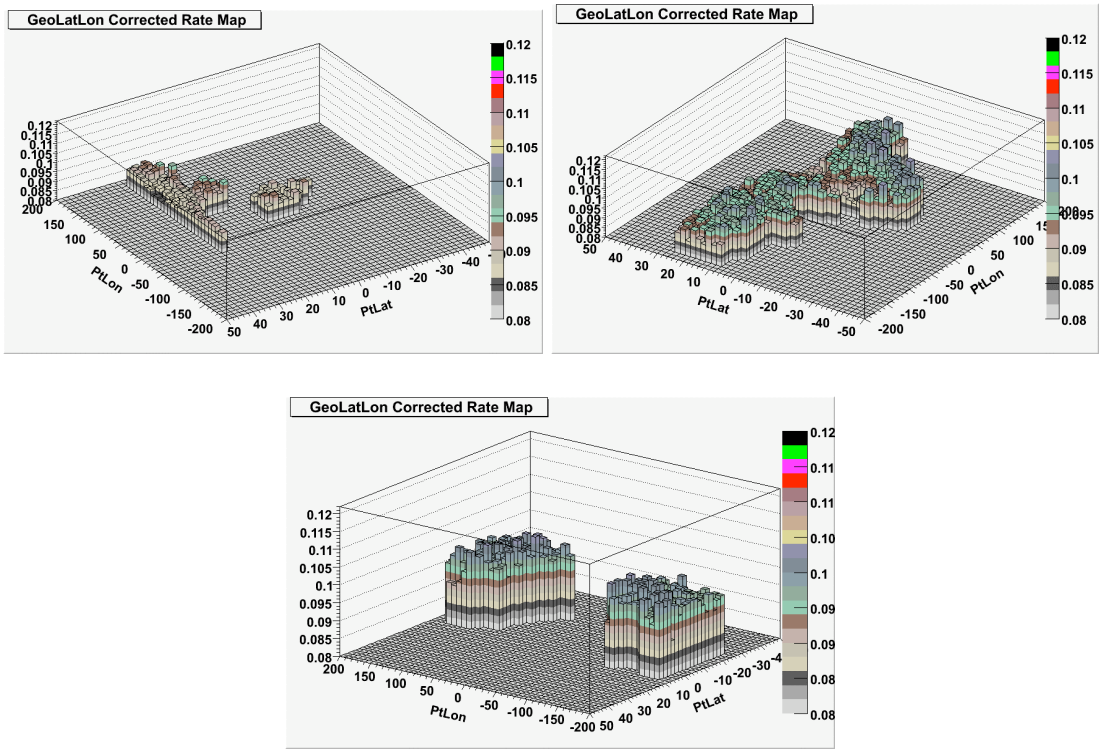

Figure 19: The location of the low (top left), medium (top right) and high (bottom) rate regions.

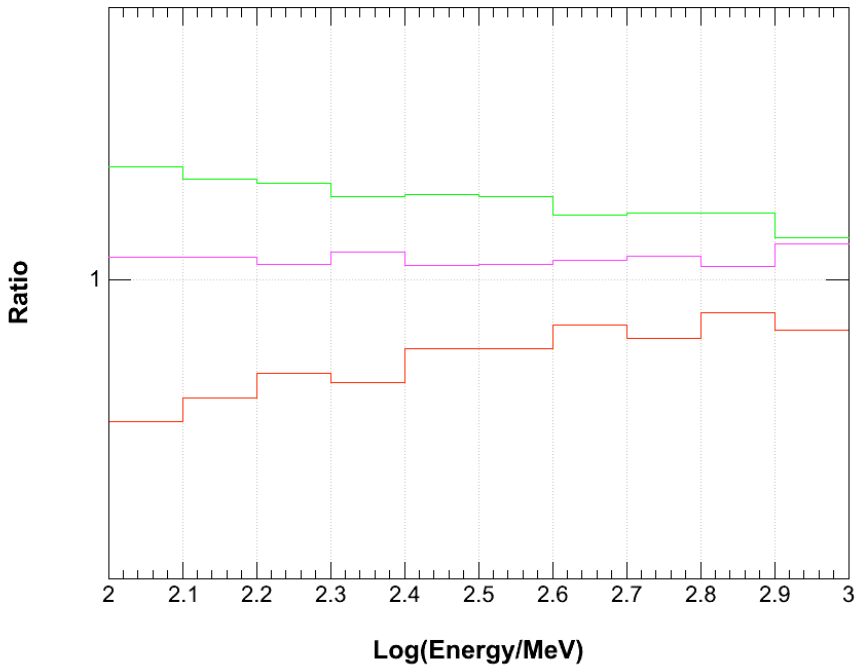

Figure 20: Relative energy spectra for the low (red curve), medium (purple curve) and high (green curve) rate regions.

—

Effects of 2% maximum amplitude might be expected if these regions were looking at much different parts of the sky. The low rate region has the fewest particles at all energies and the effect increases towards the lower energies. The size of the effect is at a maximum of 5% between 100 and 125 MeV.

Discussion and Conclusions: The data selections have resulted in rates of about 0.1 Hz given the data selections I have used. The statistical precision for most of this analysis is in the range of 0.001-0.002 Hz. Effects of rate differences in the range of 5% or 0.005 Hz are observed. The effects are energy dependent and are reasonably attributed not to the sky itself but to instrumental effects, probably background. As hypothesized, the effect is a function of location on the orbit from which observations were made. However, it is not clearly associated with any

specific particle population.

The effect appears at first glance to be largest when the satellite comes out of the SAA moving towards the northeast. One suggested cause is that there could be some loss of events due to activation of either the CsI crystals or the ACD tiles during their SAA passage, which then decays away on a roughly a ¼ orbit timescale. While such activation effects are seen in the count rates from individual detector channels, there are several reasons I do not think this is the explanation. First, the low rate region(s) is(are) not the same at all energies. Second the lowest rate region appears to have two parts (see Figure 19), one almost adjacent to the SAA and one further to the northeast. Third, at high energies the low rate region is seen at high latitudes.

Summary of findings:

1) The high latitude sky can be used as a standard candle that, when integrated over several orbital precession periods, will illuminate the Fermi Large Are Telescope (LAT) uniformly with photons.

2) McIlwain B and L parameters are good proxies for the magnetic cutoff and can be used as independent variables to study and correct for rate dependent efficiencies.

3) The Pass 6 analysis of the LAT data, augmented with additional background rejections cuts developed for the high latitude extragalactic diffuse emission, allows study of any residual background associated with the location of the satellite in the near Earth environment.

4) There is excess of background near the boundaries of the SAA that is not removed by the augmented Pass 6 cuts.

5) There appears to be a component of energy dependent background associated with some regions on the orbit. Consequently, there are regions on the orbit where lower background observations can be made.

In conclusion, I can say there are regions of the orbit from which lower

background observations can be made. I recommend that some background-limited sources be observed from those regions identified in this report.

References:

Abdo et al., 2010a, Phys Rev Lett, 104, 101101.
Abdo et al., 2010b, ApJS, 188, 405.
Alcaraz, J. et al., 2000, Physics Letters B **484**, 10.
Charles, E., (on behalf of the Fermi LTA Collaboration), 2009, "*Particle Background Effects on Efficiency and Residual Background Contamination in the LAT Diffuse Class Photon Sample*", Fermi Symposium poster paper.

Cohen, de Rujula and Glashow, 1998, ApJ, **495**, 639.
Derome, L., Bu´enerd, M., and Liu, Y., 2001, arXiv:astro_ph/0103474.
Dmitriev, A. V., et al., 1998, Adv. in Space Res., **21**, No. 12, 1797.
Gehrels and Michelson, 1999, *Gamma-ray Large Area Space Telescope Science Requirements Document*, http://fermi.gsfc.nasa.gov/science/resources/aosrd/.
Honda, M., 2009, private commnication.
Honda, M., et al., 2007, Phys. Rev. D **75**, 043006.
Kniffen et al., 1996, A&A Suppl. **120**, 615.
Kolb, E. W. and Turner, M. S., 1983, Ann. Rev. of Nuc. and Particle Science, **33**, 645.
Mikhailov, 2002, J. of Mod. Phys. A, March 25, 2002, 107.
Mohapatra, R. N. 2003, *Unification and Supersymmetry: The Frontiers of Quark-Lepton Physics*, Published by Springer, ISBN 0387955348, 9780387955346.
Moskalenko et al., 2008, ApJ, **681**, 1708.
Ormes, presentation made at GSFC June 14, 2010, appended to this report.
Sanuki, T., et al., 2007, Phys. Rev. D **75**, 043005.
Stecker, F. W., 2003, Proc. Conf. Matter-Antimatter Asymmetry, arXiv:hep-ph/0207323.
Stecker, Hunter and Kniffen, 2008, Astroparticle Phys. **29**, 25.
Steigman, G. 1976, ARA&A, **14**, 339.
Strong, Moskalenko and Reimer, 2004, ApJ **613**, 956.
Sreekumar et al., 1998, ApJ **494**, 523.
Voronov, S.A., A.M. Galper, S.V. Koldashov, L.V. Maslennikov, V.V. Mikhailov, and A.V. Popov, 1991, Cosmic Res., Engl. Transl., **29**(4), 567.
P. Zuccon, P., et al., 2003, Proc. 28th ICRC, Tsukuba, 2003.